THEORETICA CHIMICA ACTA

Theoret. Chim. Acta (Berl.) 61, 87–101 (1982)

Diatomic Interactions in Momentum Space. The $2p\pi_u$ and $3d\pi_g$ States of H_2^+ System

Toshikatsu Koga*, Minoru Sugawara, and Mutsuo Morita

Departments of Industrial Chemistry and of Applied Science for Energy, Muroran Institute of Technology, Muroran, Hokkaido, 050 Japan

The recently proposed method of momentum electron density for interatomic interactions is applied to the two π states of the H_2^+ system. The processes of the attractive $2p\pi_u$ and repulsive $3d\pi_g$ interactions are analysed based on the behaviour of the momentum density and Compton profile. The results are compared with the previous ones for the $1s\sigma_g$ and $2p\sigma_u$ states. The guiding principle of contraction and expansion for the energy-density relation in momentum space is shown to be common to both the σ and π states.

Key words: Momentum electron density – Compton profile – H_2^+ System – π States of $\sim$.

1. Introduction

In the early 1940s, an investigation of the chemical bond from the momentum (p-) space viewpoint was initiated by Coulson and Duncanson [1] based on the Dirac–Fourier transform [2] of the coordinate (r-) space wave function. Though the wave functions they employed were far less accurate than those available today, they [1] gave in a series of papers some significant insight into the p-space characteristics of the chemical bonding not only in diatomic H_2^+ and H_2 molecules but also in simple hydrocarbons. However, the p-space treatment has received little attention in molecular quantum mechanics, partly because our everyday intuition is more confined to a space of lengths rather than that of velocities. The momentum electron density $\rho(\mathrm{p})$, which is a basic physical quantity in our present approach, has been examined only in relation to the Compton profiles

* To whom all correspondence should be addressed

0040-5744/82/0061/0087/$03.00

of atoms and molecules at their equilibrium conformations. However, the r- and p-representations are complementary to one another [2], and a study in p-space is expected to provide a new or alternative understanding to the bonding problem.

Indeed, there seems to be renewed interests on the use of p-space concept for several atomic and molecular phenomena in recent years [3]. Especially, we have recently proposed a method of momentum density for interatomic interactions [4] which permits to clarify the origin of nuclear rearrangements (such as molecular geometries and chemical reactions) in terms of the concept in p-space instead of the usual one in r-space. Considering a uniform scaling process of an arbitrary molecular conformation R_0 with scaling factor s, we have shown that the difference in momentum density $\rho(\mathsf{p})$ and its modified forms defined by

$$\Delta\rho(\mathsf{p}; s) \equiv \rho(\mathsf{p}; s) - \rho(\mathsf{p}; \infty), \tag{1a}$$

$$\Delta\bar{\rho}(\mathsf{p}; s) \equiv (1/s) \int_s^\infty ds' \, \Delta\rho(\mathsf{p}; s'), \tag{1b}$$

$$\Delta\tilde{\rho}(\mathsf{p}; s) \equiv \Delta\bar{\rho}(\mathsf{p}; s) + \Delta\rho(\mathsf{p}; s), \tag{1c}$$

rigorously govern kinetic energy, stabilization energy, and interatomic force of the system, respectively. It has been then suggested that the contraction and expansion observed in these density differences are important concept which characterizes the nature of nuclear rearrangements in p-space. The method has been applied to the two lowest σ states of the H_2^+ system [5]. For the attractive $1s\sigma_g$ and repulsive $2p\sigma_u$ interactions, the behaviour of momentum density and its effect on the energy and force have been quantitatively examined. Origin of covalent bonding has been also discussed based on the energy partitionings proposed previously [4].

The purpose of this paper is to extend the application of the momentum density approach to the π states of the H_2^+ system. For the bonding $2p\pi_u$ and antibonding $3d\pi_g$ states, the reorganization of $\rho(\mathsf{p})$ and its effect on the stabilization/destabilization of the system are quantitatively investigated in comparison with the previous results for the $1s\sigma_g$ and $2p\sigma_u$ states. In the next section, the present theory of momentum density is outlined, and the results are discussed in Sec. 3. Sec. 3.1 provides discussion on the differences between σ/π and bonding/antibonding states in p-space on the basis of the momentum density distributions and Compton profiles. The behaviour of momentum density and its energetic contribution during the interaction processes are analysed in Sec. 3.2. Atom–bond partitioning is also examined. Changes in the average and directional Compton profiles and the parallel-perpendicular partitioning of the stabilization energy are discussed in Sec. 3.3.

2. Theoretical Ground

For diatomic systems, the scale factor s in Eq. (1a–c) can be replaced with internuclear distance R. Then the density differences $\Delta\rho(\mathsf{p}; R)$, $\Delta\bar{\rho}(\mathsf{p}; R)$, and

$\Delta\tilde{\rho}(\mathbf{p}; R)$ are rigorously related with the kinetic energy $\Delta T(R)$ [$\equiv T(R) - T(\infty)$], stabilization energy $\Delta E(R)$ [$\equiv E(R) - E(\infty)$], and interatomic force $F(R)$ [$\equiv -dE(R)/dR$] of the system respectively by [4]

$$\Delta T(R) = \int d\mathbf{p}(p^2/2)\Delta\rho(\mathbf{p}; R), \tag{2a}$$

$$\Delta E(R) = \int d\mathbf{p}(p^2/2)\Delta\bar{\rho}(\mathbf{p}; R), \tag{2b}$$

$$F(R) = (1/R) \int d\mathbf{p}\,(p^2/2)\Delta\tilde{\rho}(\mathbf{p}; R), \tag{2c}$$

where $p = |\mathbf{p}|$. These relations are deduced from the virial theorem and hence the validity of the theorem is necessary condition for Eq. (2a–c). In order to conserve the number of electrons, the three density differences must satisfy

$$\int d\mathbf{p}\,\Delta\rho(\mathbf{p}; R) = \int d\mathbf{p}\,\Delta\bar{\rho}(\mathbf{p}; R) = \int d\mathbf{p}\,\Delta\tilde{\rho}(\mathbf{p}; R) = 0 \tag{3}$$

for any value of R.

Based on Eq. (2) under the condition (3), we can derive some guiding principle for the effect of the density reorganization in p-space on the energy and force of a system [4]: Negative ΔT, ΔE, and F are possible only when the corresponding $\Delta\rho$, $\Delta\bar{\rho}$, and $\Delta\tilde{\rho}$ show contraction, i.e. a reorganization of momentum density which results in a density increase at lower momentum with a simultaneous decrease at higher momentum. On the contrary, positive energies and force result only when the momentum densities reveal expansion, i.e. a density reorganization reverse to the contraction. Therefore, it is, for example, concluded that the contraction of $\Delta\rho$ at larger R predicts formation of stable chemical bonds since the behaviours of ΔT and ΔE are parallel in the initial stage of interactions [4]. At equilibrium separations (R_e), expansion of $\Delta\rho$, maximum contraction of $\Delta\bar{\rho}$, and critical behaviour of $\Delta\tilde{\rho}$ should be observed. On the other hand, monotonous expansion of $\Delta\rho$, $\Delta\bar{\rho}$, and $\Delta\tilde{\rho}$ against R implies that the interaction is repulsive and no stable bond is formed.

Since the kinetic operator $(p^2/2)$ appeared in the basic Eqs. (2a–c) is angular-independent, Eqs. (1–3) can be rewritten by using the radial momentum density

$$I(p; R) = \int_0^{2\pi} d\phi_p \int_0^{\pi} d\theta_p\, p^2 \sin\theta_p \rho(\mathbf{p}; R), \tag{4}$$

and the resultant differences in radial density, $\Delta I(p; R)$, $\Delta\bar{I}(p; R)$, and $\Delta\tilde{I}(p; R)$ [5]. These radial densities reduce the required density information from the three-dimensional $\rho(\mathbf{p})$ to the one-dimensional $I(p)$ without loss of generality and exactness of the approach. Use of $I(p)$ connects the present approach with the experimental Compton profiles in a direct manner: Within the impulse approximation, the spherically-averaged intensity of Compton scattering is given

by [3]

$$J(q;R)=(1/2)\int_{|q|}^{\infty} dp\, p^{-1} I(p;R). \tag{5a}$$

Thus the change in Compton profile from separated atoms to molecule is

$$\Delta J(q;R)\equiv J(q;R)-J(q;\infty)$$
$$=(1/2)\int_{|q|}^{\infty} dp\, p^{-1}\Delta I(p;R), \tag{5b}$$

and hence ΔJ and ΔI must show parallel behaviour at a given R. At stable equilibrium, for instance, the half-width of Compton profile should be larger than that of separated atoms, since ΔI and then ΔJ expand at this conformation.

Based on Eqs. (2a–c), we can decompose the energy and force into several components which have some physical images [4]. If the parent wave function employed is in an LCAO form, momentum densities $\rho(\mathrm{p})$ and $I(p)$ are separated into one-center atomic and two-center interatomic (bond) parts. Then, we can distinguish ΔT, ΔE, and F into atomic and interatomic contributions. Directional partitioning is also possible which results from the decomposition of the kinetic operator into the parallel and perpendicular parts. The latter partitioning is closely related with the directional Compton profile, e.g. $T_{\parallel}(R)=\int_{-\infty}^{+\infty} dp_{\parallel}\,(p_{\parallel}^2/2)J_{\parallel}(p_{\parallel};R)$ where $J_{\parallel}(p_{\parallel};R)=\int_{-\infty}^{+\infty} dp_{\perp}\int_{-\infty}^{+\infty} dp_{\perp'}\rho(p_{\parallel},p_{\perp},p_{\perp'};R)$ is the profile of Compton scattering along the molecular axis. Details of these energy partitionings are given in Ref. [4, 5].

3. Behaviour of Momentum Density and Its Energetic Contribution

3.1. Shapes of Momentum Density Distribution and Compton Profile

In the LCAO approximation, the r-space wave function for the $2p\pi_u$ and $3d\pi_g$ states of the H_2^+ system is given by

$$\psi(\mathrm{r})=(2\pm 2S)^{-1/2}\{\chi_A(\mathrm{r})\pm\chi_B(\mathrm{r})\}, \tag{6a}$$

where S is the overlap integral. In Eq. (6a) and hereafter, addition and subtraction represent the $2p\pi_u$ and $3d\pi_g$ states, respectively. Since the choice of single $2p\pi$ AO for $\chi(\mathrm{r})$ (i.e. Finkelstein–Horowitz type wave function [6]) yields poor results for the present states[1], we here adopt the Dickinson type wave function [7] which consists of $2p\pi$ and $3d\pi$ AOs having the same orbital exponent ζ. That is

$$\chi_A(\mathrm{r})=c_1 2p\pi_A(\mathrm{r})+c_2 3d\pi_A(\mathrm{r}), \tag{6b}$$

[1] For the $2p\pi_u$ state, the equilibrium distance and dissociation energy (R_e, D_e) in atomic units are (8.82, 0.00218) in the Finkelstein–Horowitz approximation and (8.06, 0.00805) in the Dickinson approximation, while the exact values are (7.96, 0.00951). When D_e is used as a measure, the previous results for the $1s\sigma_g$ state [5] based on the Finkelstein–Horowitz wave function are of 85% accuracy. In order to attain a comparable accuracy, the Dickinson type wave function is required in the $2p\pi_u$ state.

$$2p\pi_A(\mathbf{r}) = 2(3^{-1/2})\zeta^{5/2}|\mathbf{r}-\mathbf{R}_A| \exp(-\zeta|\mathbf{r}-\mathbf{R}_A|) Y_{1,m}(\theta, \phi), \tag{6c}$$

$$3d\pi_A(\mathbf{r}) = 2^{3/2}3^{-1}5^{-1/2}\zeta^{7/2}|\mathbf{r}-\mathbf{R}_A|^2 \exp(-\zeta|\mathbf{r}-\mathbf{R}_A|) Y_{2,m}(\theta, \phi), \tag{6d}$$

where $m = \pm 1$, $\mathbf{R}_A$ the position of nucleus A ($R = |\mathbf{R}_A - \mathbf{R}_B|$), and $Y_{l,m}(\theta, \phi)$ the spherical harmonics. The exponent ζ and coefficients c_1 and c_2 are variationally optimized at every R and this guarantees the validity of the virial theorem and therefore the basic Eqs (2a–c) of the present approach.

The Fourier transform [2] of (6a–d) gives the corresponding p-space wave function [8]

$$\psi(\mathbf{p}) = (2 \pm 2S)^{-1/2}\{\chi_A(\mathbf{p}) \pm \chi_B(\mathbf{p})\}, \tag{7a}$$

$$\chi_A(\mathbf{p}) = \exp(-i\mathbf{p} \cdot \mathbf{R}_A)\{c_1 2p\pi(\mathbf{p}) + c_2 3d\pi(\mathbf{p})\}, \tag{7b}$$

$$2p\pi(\mathbf{p}) = -i2^{9/2}3^{-1/2}\pi^{-1/2}\zeta^{7/2}p(p^2+\zeta^2)^{-3} Y_{1,m}(\theta_p, \phi_p), \tag{7c}$$

$$3d\pi(\mathbf{p}) = -2^6 5^{-1/2}\pi^{-1/2}\zeta^{9/2}p^2(p^2+\zeta^2)^{-4} Y_{2,m}(\theta_p, \phi_p). \tag{7d}$$

Then the momentum electron density $\rho(\mathbf{p})$ is

$$\rho(\mathbf{p}) = \rho_{\text{atom}}(\mathbf{p}) + \rho_{\text{bond}}(\mathbf{p}), \tag{8a}$$

$$\rho_{\text{atom}}(\mathbf{p}) = (1 \pm S)^{-1}\{c_1^2 2^6 \pi^{-2}\zeta^7 p^2(p^2+\zeta^2)^{-6} \sin^2\theta_p + c_2^2 2^9 3\pi^{-2}\zeta^9 p^4(p^2+\zeta^2)^{-8} \sin^2\theta_p \cos^2\theta_p\}, \tag{8b}$$

$$\rho_{\text{bond}}(\mathbf{p}) = \pm(1 \pm S)^{-1}\{c_1^2 2^6 \pi^{-2}\zeta^7 p^2(p^2+\zeta^2)^{-6} \sin^2\theta_p \cos(pR\cos\theta_p) + c_1 c_2 2^{17/2}3^{1/2}\pi^{-2}\zeta^8 p^3(p^2+\zeta^2)^{-7} \sin^2\theta_p \cos\theta_p \sin(pR\cos\theta_p) - c_2^2 2^9 3\pi^{-2}\zeta^9 p^4(p^2+\zeta^2)^{-8} \sin^2\theta_p \cos^2\theta_p \cos(pR\cos\theta_p)\}, \tag{8c}$$

and the radial momentum density $I(p)$ results in

$$I(p) = I_{\text{atom}}(p) + I_{\text{bond}}(p), \tag{9a}$$

$$I_{\text{atom}}(p) = (1 \pm S)^{-1}\{c_1^2 2^9 3^{-1}\pi^{-1}\zeta^7 p^4(p^2+\zeta^2)^{-6} + c_2^2 2^{12}5^{-1}\pi^{-1}\zeta^9 p^6(p^2+\zeta^2)^{-8}\}, \tag{9b}$$

$$I_{\text{bond}}(p) = \pm(1 \pm S)^{-1}\{c_1^2 2^9 \pi^{-1}\zeta^7 p^2(p^2+\zeta^2)^{-6}R^{-2}[(\sin pR)/pR - \cos pR] + c_1 c_2 2^{23/2}3^{1/2}\pi^{-1}\zeta^8 p^3(p^2+\zeta^2)^{-7}R^{-2} \times[-3(\cos pR)/pR + (3/p^2R^2 - 1)\sin pR] - c_2^2 2^{12}3\pi^{-1}\zeta^9 \times p^3(p^2+\zeta^2)^{-8}R^{-3}[(12/pR - pR)\cos pR + (5 - 12/p^2R^2)\sin pR]\}, \tag{9c}$$

where spherical coordinates (p, θ_p, ϕ_p) are used for $\mathbf{p}$ with the p_z-axis parallel to the molecular axis.

Typical profiles of $\rho(\mathbf{p})$, $I(p)$, and $J(q)$ are respectively shown in Figs. 1, 2a, and 2b. The figures also include the results for the σ states [5] for comparison.

[2] The coefficients c_1 and c_2 in (6b) satisfy $c_1^2 + c_2^2 = 1$ from the normalization of AO.

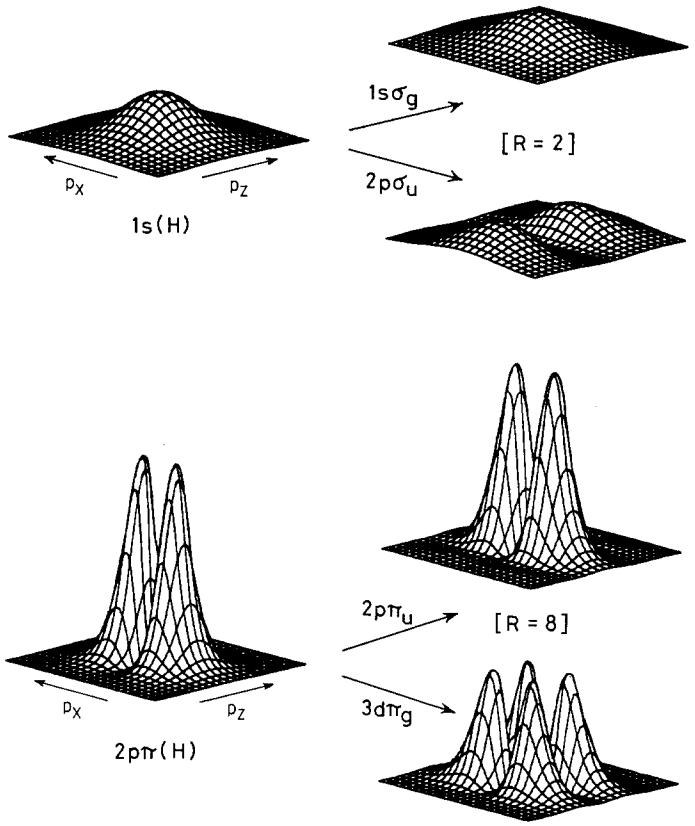

Fig. 1. Perspective plots of momentum electron density distribution for the σ and π states of the H_2^+ system. These plots are drawn for the region $-1 \leq p_x < 1$ and $-1 \leq p_z \leq 1$ in the same scale from the same visual point. All values are given in atomic units

The Compton profiles $J(q)$ have been calculated numerically applying the Gauss integration formula [9] to Eqs. (5a) and (9a–c).

In Fig. 1, the directional character of $\rho(\mathbf{p})$ is shown to be same to that of $\rho(\mathbf{r})$, the electron density in r-space, since the Fourier transform does not change the angular part of AO (see Eqs. (6) and (7)). The momentum densities for the π states have a nodal plane parallel to the bond (p_z) axis, while those for the σ states do not. In addition, the densities for the $3d\pi_g$ and $2p\sigma_u$ states have a node perpendicular to the p_z axis due to the antibonding nature. In Figs. 1 and 2a, $\rho(\mathbf{p})$ and $I(p)$ have sharper and higher peaks near the origin for the π states than for the σ states. The same trend is observed in $J(q)$ depicted in Fig. 2b. This means that the π density is more contracted than the σ density in p-space and therefore electron has smaller kinetic energy in the π states. Since the r- and p-space wave functions of a system emphasize inverse regions of the respective spaces [3], the contracted nature of the π density in p-space is a direct reflection of the delocalized and diffusive nature of the density in r-space. When

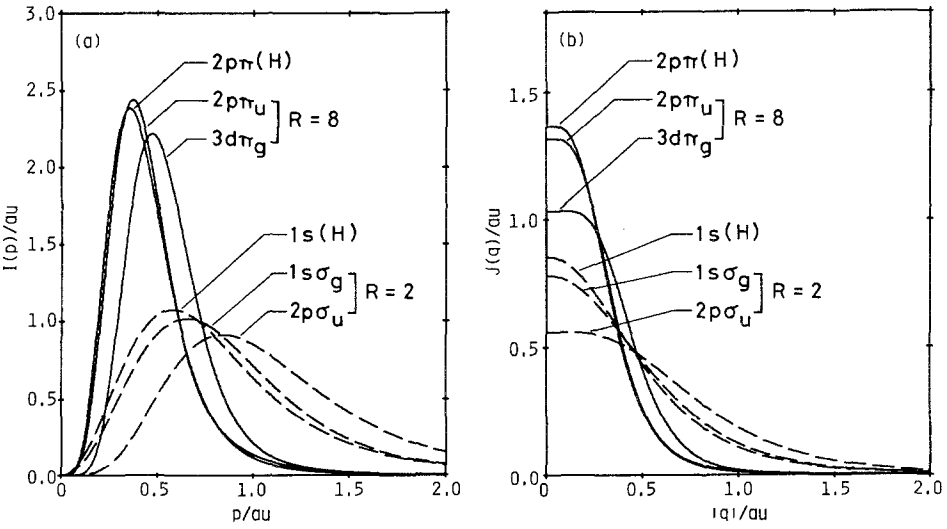

Fig. 2. Radial momentum electron density distributions $I(p)$ and average Compton profiles $J(q)$

compared to the results for the isolated atoms, the momentum densities expand in the molecule with a simultaneous increase in the kinetic energy. In Fig. 2a, the position of peak is a good measure of the degree of expansion; the expansion increases in the order of $2p\pi(\mathrm{H}) < 2p\pi_u < 3d\pi_g \ll 1s(\mathrm{H}) < 1s\sigma_g < 2p\sigma_u$. The order of expansion also holds for $J(q)$ in Fig. 2b and $J(0)$ is a good measure in this case. (Note that $J(0)$ is just half the expectation value $\langle p^{-1} \rangle$ from Eq. (5a).) These observations exemplify the predicted parallelism between the behaviours of $I(p)$ and $J(q)$ (see Sec. 2).

3.2. Behaviour of Momentum Density

We here examine the behaviour of momentum density and its effect on the energy and force of the system during the processes of attractive and repulsive interactions. For the sake of simplicity, we proceed with our study using the radial density distribution. The difference ΔI is immediately obtained from Eq. (9) by subtracting the hydrogen-atomic $2p\pi$ density $I_{2p\pi}(p) = (4/3\pi)p^4(p^2+1/4)^{-6}$. The modified differences $\Delta\bar{I}$ and $\Delta\tilde{I}$ are numerically calculated using the Gauss and Filon integration formulas [9]. These density differences for the $2p\pi_u$ state are given in Fig. 3 for several R, and the resultant ΔT and ΔE curves are shown in Fig. 4 together with their atom-bond and parallel-perpendicular partitionings. The curves for F and its components are not given since they are merely the gradients of the corresponding ΔE and its components. Figs. 5 and 6 summarize the results for the repulsive $3d\pi_g$ state.

In the $2p\pi_u$ state (Figs. 3 and 4), the ΔI plots initially show contraction ($R = 20$ and 12 a.u.) and then expansion ($R = 8$ and 6 a.u.). (The expansion at $R = R_e$ is also observed in Figs. 1 and 2a.) The contraction at large separations reflects the r-space concept of the delocalization of electron density or the enlargement

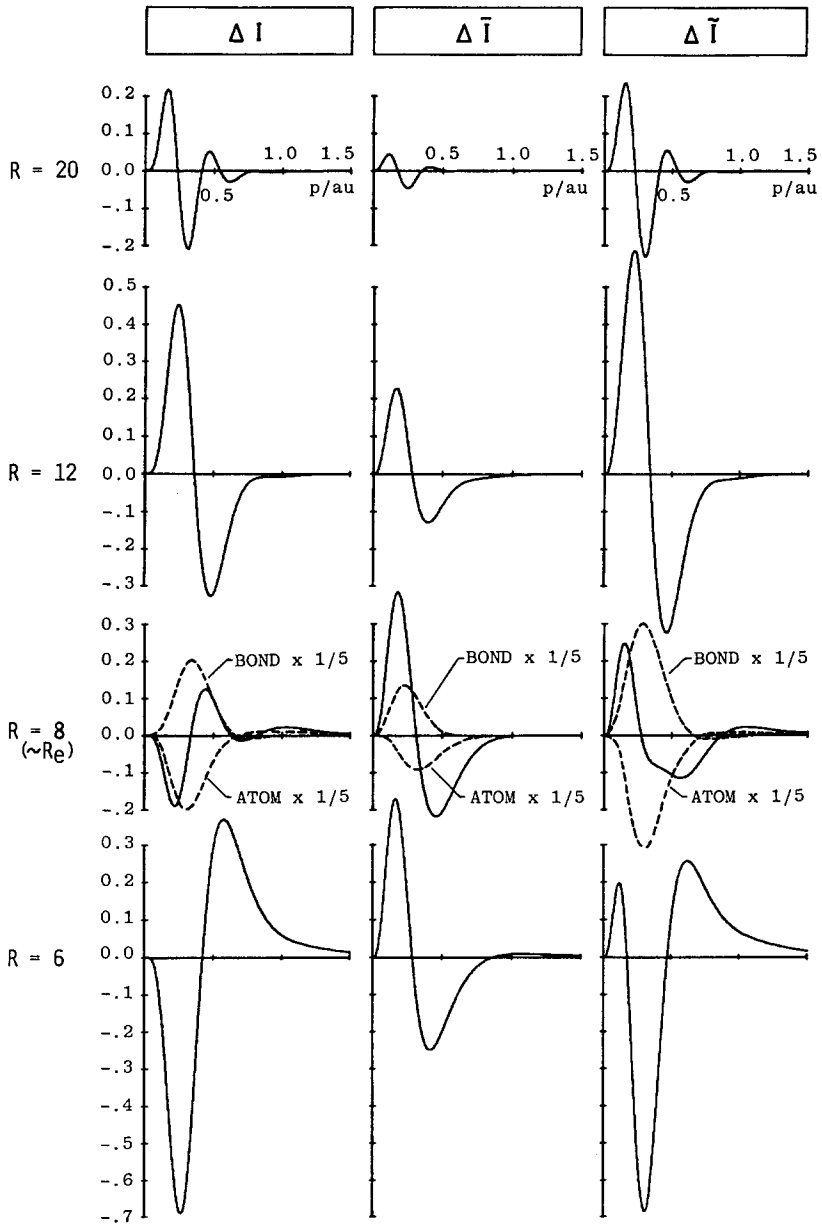

Fig. 3. The $2p\pi_u$ state. Differences in the radial momentum density distributions. The ΔI, $\Delta \bar{I}$, and $\Delta \tilde{I}$ govern ΔT, ΔE, and F, respectively. All values are given in atomic units

of the space of electron motion, while the expansion at small separations reflects the increased localization of the r-space density around the two nuclei. These reorganizations of momentum density result in negative and positive ΔT, respectively, and the critical point is calculated to be $R = 9.1$ a.u. where ΔT vanishes

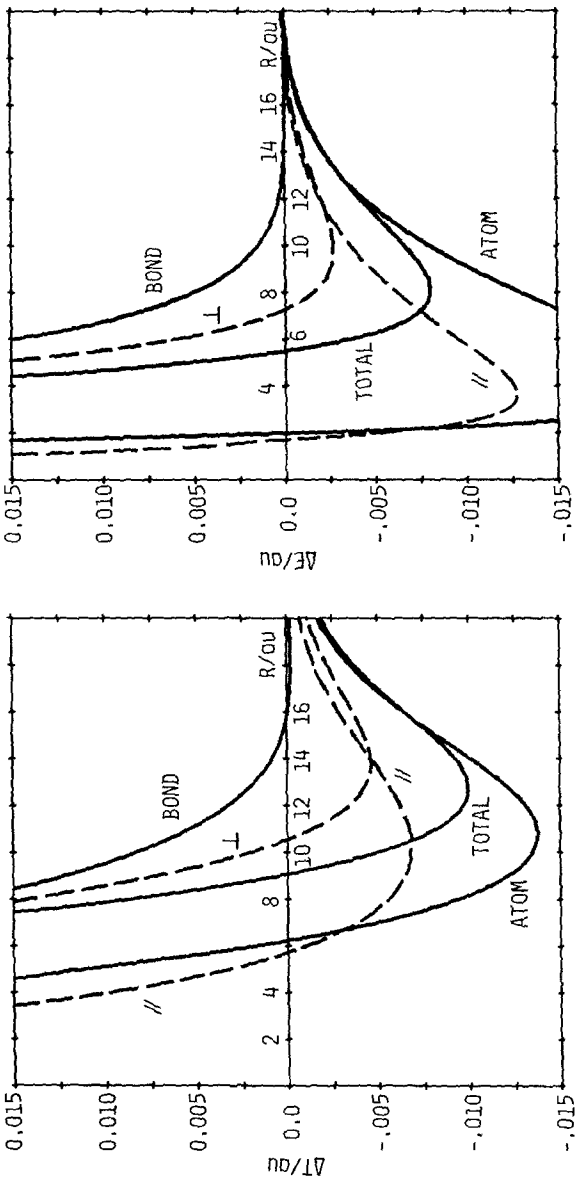

13129 **Fig. 4.** The $2p\pi_u$ state. Kinetic and stabilization energies obtained from the momentum density. Their decompositions into the atom-bond and the parallel-perpendicular components are also shown

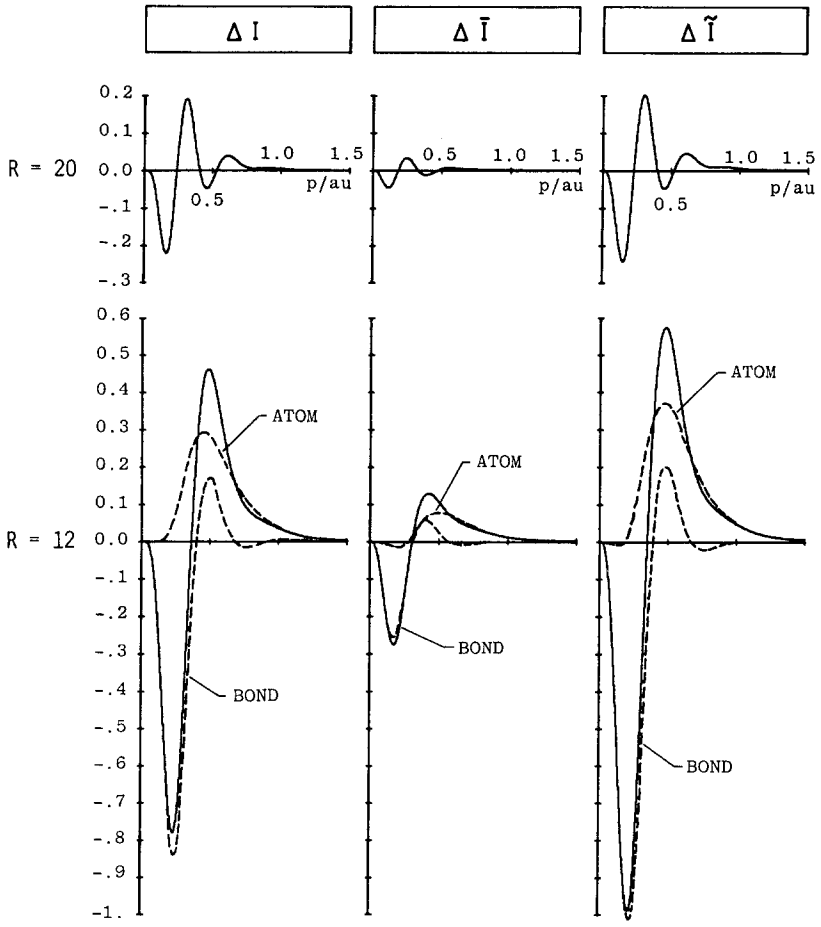

Fig. 5. The $3d\pi_g$ state. See the captions to Fig. 3

(see Fig. 4). According to the guiding rule, the initial contraction and final expansion of the difference density ΔI predict the presence of a stable bond in this state, which will be clarified by the examination of $\Delta\bar{I}$ and $\Delta\tilde{I}$ plots. The difference $\Delta\bar{I}$ in Fig. 3 shows contraction for $R \geq 8$ a.u. and its magnitude increases as R decreases. This implies negative ΔE and increasing stability of the system up to 8 a.u. At $R = 6$ a.u., however, an expansive nature appears at a large p-region ($p > 0.87$ a.u.) which cancels in part the contraction. This corresponds to the turning up of the ΔE curve for $R < R_e$ (see Fig. 4). The modified difference $\Delta\tilde{I}$, which is the origin of the interatomic force F, shows contraction for $R = 20$ and 12 a.u. and expansion for $R = 6$ a.u. For $R_e = 8$ a.u., it reveals both the contraction at small p and expansion at large p. When the weighting factor ($p^2/2$) is taken into account, their contributions are shown to be in the same magnitude and there is no total contribution. The resultant force is attractive ($F < 0$) for $R \geq 12$ a.u., zero for $R_e = 8$ a.u., and repulsive ($F > 0$) for $R = 6$ a.u., in accordance with the result of the ΔE curve.

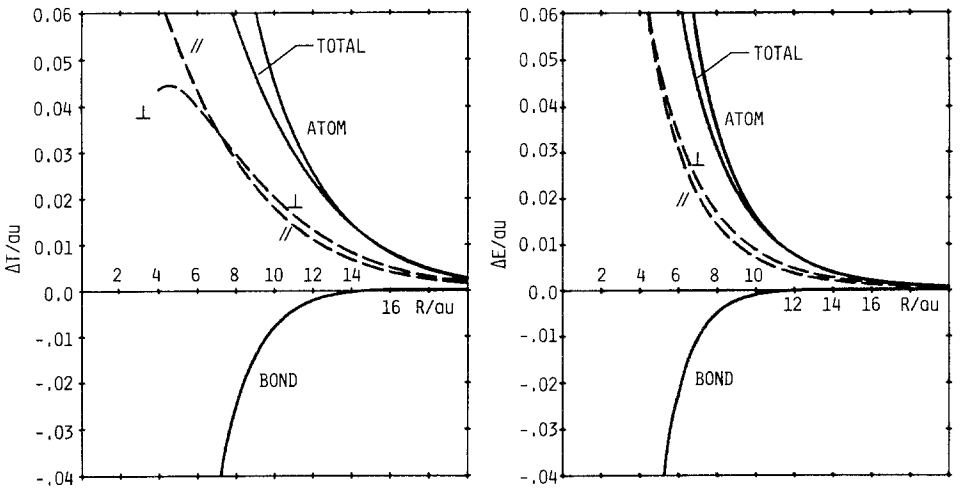

Fig. 6. The $3d\pi_g$ state. See the captions to Fig. 4

In the $3d\pi_g$ state, all the momentum densities ΔI, $\Delta \bar{I}$, and $\Delta \tilde{I}$ given in Fig. 5 show expansion whose degree increases rapidly as R decreases. In the antibonding state, the existence of the nodal plane $p_z = 0$ prohibits the density from distributing in the low-momentum region around the origin, leading to the expansion of momentum density (see Fig. 1). The corresponding picture in r-space is that the electron is confined to a narrower space in molecular system than in free atoms due to the r-space node which bisects the molecular axis. These expansions are responsible for monotonous increases of ΔT, ΔE, and F (Fig. 6), meaning that no stable bonds are formed in this state.

The proposed guiding principle [4] for the relation between the reorganization of momentum density and its effect on the energy and force of a system are thus shown to be valid and common to both the σ and π states.

The results for the atom-bond partitioning also show the same trend as those of the σ states. In the bonding $2p\pi_u$ state, the density flows from the one-center atomic to the two-center bond part (see dashed lines for $R = 8$ a.u. in Fig. 3). The decrease in the atomic density causes a decrease of the kinetic pressure in this part, which predominantly contributes to lower the kinetic and total energies (Fig. 4). The atomic part is important to initiate and accelerate the reaction, while the bond part is to terminate the reaction. In the $3d\pi_g$ state, the density flows in the opposite way (Fig. 5) and the kinetic pressure increases in the atomic part. As a result, the atomic part is the predominant origin of the destabilization of the system (Fig. 6).

3.3. Behaviour of Average and Directional Compton Profiles

In this subsection, the behaviours of Compton profiles are examined. The parallel-perpendicular partitioning of the stabilization energy is also discussed

based on the directional Compton profiles. The average profile is obtained by substituting the radial momentum density (9) into (5a), while the directional profiles are given by

$$J_{\parallel}(p_{\parallel}) = (1 \pm S)^{-1}\{c_1^2 2^4 5^{-1}\pi^{-1}\zeta^7 z_1^{-4}(1 \pm \cos p_{\parallel}R)$$
$$\pm c_1 c_2 2^{15/2} 3^{-1/2} 5^{-1}\pi^{-1}\zeta^8 p_{\parallel} z_1^{-5} \sin p_{\parallel}R$$
$$+ c_2^2 2^8 7^{-1}\pi^{-1}\zeta^9 p_{\parallel}^2 z_1^{-6}(1 \mp \cos p_{\parallel}R)\}, \tag{10a}$$

$$J_{\perp}(p_{\perp}) = (1 \pm S)^{-1}\{c_1^2 5^{-1}\pi^{-1}\zeta^7[2^6 p_{\perp}^2 z_2^{-5} + 2^3 z_2^{-4}$$
$$\pm 6^{-1}(p_{\perp}^2 z_2^{-5/2} R^5 K_5(z_3) + z_2^{-2} R^4 K_4(z_3))]$$
$$\pm c_1 c_2 2^{-1/2} 3^{-3/2} 5^{-1}\pi^{-1}\zeta^8[z_2^{-2} R^5 K_4(z_3) + p_{\perp}^2 z_2^{-5/2} R^6 K_5(z_3)]$$
$$+ c_2^2 7^{-1}\pi^{-1}\zeta^9[2^6 5^{-1} z_2^{-5} + 2^7 p_{\perp}^2 z_2^{-6} \mp 30^{-1}(11 z_2^{-5/2} R^5 K_5(z_3)$$
$$+ (12 p_{\perp}^2 - \zeta^2) z_2^{-3} R^6 K_6(z_3) - p_{\perp}^2 z_2^{-5/2} R^7 K_7(z_3))]\}, \tag{10b}$$

$$J_{\perp'}(p_{\perp'}) = J_{\perp}(p_{\perp'}), \tag{10c}$$

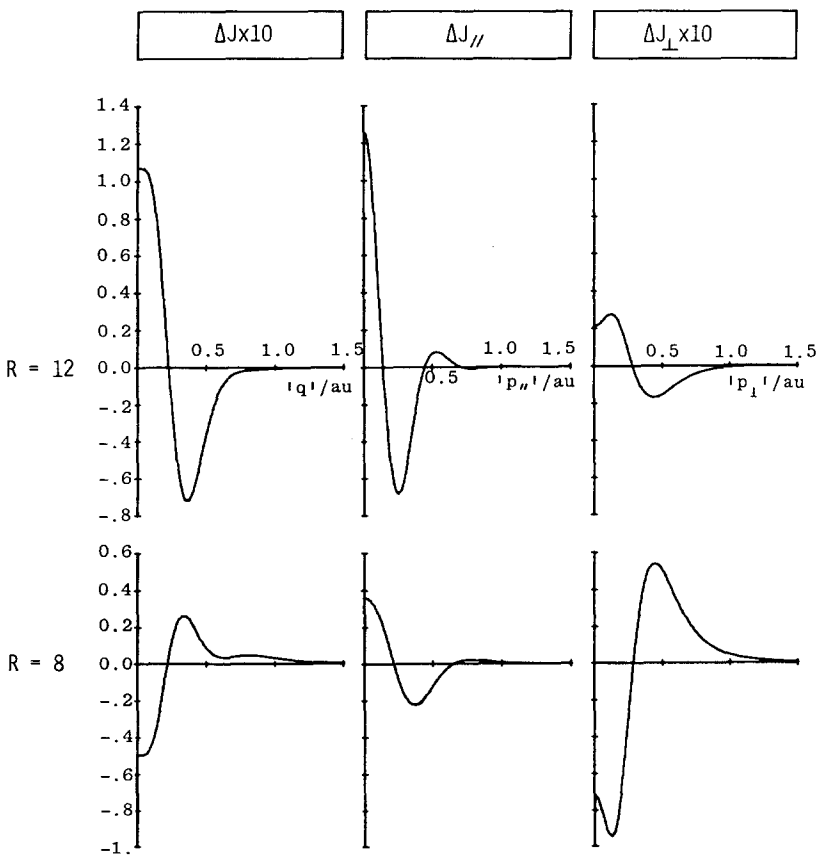

Fig. 7. The $2p\pi_u$ state. Differences in the average and directional Compton profiles. All values are given in atomic units

where $z_1 = (p_\parallel^2 + \zeta^2)$, $z_2 = (p_\perp^2 + \zeta^2)$, $z_3 = R(p_\perp^2 + \zeta^2)^{1/2}$, and $K_\nu(z)$ is the modified Bessel function.

The changes of the average, parallel, and perpendicular Compton profiles, ΔJ, $\Delta J_\parallel$, and $\Delta J_\perp$, from the isolated atoms are depicted in Fig. 7 for the $2p\pi_u$ state and in Fig. 8 for the $3d\pi_g$ state. As expected theoretically from Eq. (5b), the behaviour of the average profile ΔJ is parallel to that of ΔI (see Sec. 3.1.). Namely, in the $2p\pi_u$ state, ΔJ contracts for $R = 12$ a.u. and expands for $R = 8$ a.u. (Fig. 7), whereas in the $3d\pi_g$ state ΔJ expands monotonously (Fig. 8). These contraction and expansion in ΔJ correspond respectively to negative and positive ΔT as those of ΔI do. The parallelism between ΔJ and ΔI is also found in the σ states (Fig. 2).

The directional profiles and their energetic contributions also obey the guiding rule. In the $2p\pi_u$ state (Fig. 7), contractions are observed in both $\Delta J_\parallel$ and $\Delta J_\perp$

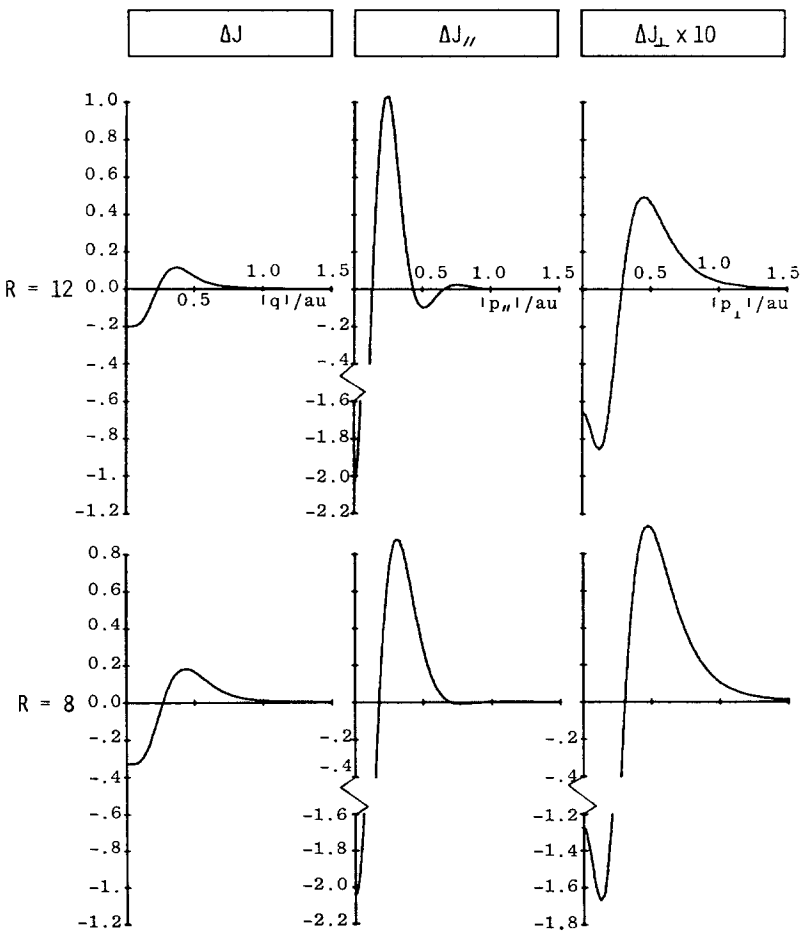

Fig. 8. The $3d\pi_g$ state. See the captions to Fig. 7

at larger separations (e.g. $R = 12$ a.u.) and therefore $\Delta E_{\parallel}$ and $\Delta E_{\perp}$ cooperatively work to stabilize the system (Fig. 4). This is mainly attributed to the extension of the space of electronic motion from atoms to molecule. A small but nonnegligible decrease in the orbital exponent also assists the contraction. At smaller separations (e.g. $R = 8$ a.u.), however, $\Delta J_{\perp}$ changes to expansion and the parallel part is a dominant origin of the stability of the molecule (i.e. $R = R_e$). The latter expansion may be due to the increased orbital exponent in this R-range which predominantly contributes to increase the kinetic pressure in the perpendicular direction. In the $3d\pi_g$ state, both the parallel and perpendicular parts expand (Fig. 8) and they cooperatively contribute to destabilize the system (Fig. 6). As mentioned before, the presence of a nodal plane $p_z = 0$ in this state works to transfer momentum density from the low momentum region around the origin to the high momentum region (see also Fig. 1). In this state, the orbital exponent increases monotonously as R decreases and the electron is bound more tightly to the nuclei in r-space. The relative importance of the directional components in the π states is slightly different from the previous one in the σ states. In the σ states, the parallel part has been shown to be of primary importance [5], but in the π states there are R-ranges where the perpendicular component dominates over the parallel one.

4. Summary

The method of momentum electron density for interatomic interactions has been applied to the $2p\pi_u$ and $3d\pi_g$ states of the H_2^+ system. The behaviours of momentum density and Compton profile have been analysed in detail during the interaction processes together with their effects on the energy and force of the system. The results have been compared with those of the $1s\sigma_g$ and $2p\sigma_u$ states studied previously. The guiding principle for the behaviour of momentum density has been shown to be valid and common to both the σ and π states. It has been also exemplified that the principle applies to the change of Compton profile during the course of interactions.

Acknowledgment. Part of this study has been supported by a Grant-in-Aid for Scientific Research from the Ministry of Education of Japan.

References

1. Coulson, C. A., Duncanson, W. E.: Proc. Camb. Phil. Soc. **37**, 55, 67, 74, 397, 406 (1941); **38**, 100 (1942); **39**, 180 (1943)
2. Dirac, P. A. M.: The principles of quantum mechanics. 4th ed. London: Oxford U.P. 1958
3. Cooper, M. J.: Adv. Phys. **20**, 453 (1971); Epstein, I. R.: Acc. Chem. Res. **6**, 145 (1973); in: International review of science. Physical chemistry. Ser. 2. Vol. 1. Theoretical chemistry. Buckingham, A. D., Coulson, C. A., ed. London: Butterworths 1975; Williams, B. G., ed.: Compton scattering. New York: McGraw-Hill 1977; Kaijser, P., Smith, Jr., V. H.: Adv. Quantum Chem. **10**, 37 (1977); Cooper, M. J.: Contemp. Phys. **18**, 489 (1977)
4. Koga, T.: Theoret. Chim. Acta (Berl.), **58**, 173 (1981)

5. Koga, T., Morita, M.: Theoret. Chim. Acta (Berl.), **59**, 423 (1981)
6. Finkelstein, B. N., Horowitz, G. E.: Z. Phys. **48**, 118 (1928); Moiseiwitsch, B. L., Stewart, A. L.: Proc. Phys. Soc. **A67**, 457 (1954)
7. Dickinson, B. N.: J. Chem. Phys. **1**, 317 (1933); Sovers, O., Kauzmann, W.: J. Chem. Phys. **35**, 652 (1961); Miller, R. L., Lykos, P. G.: J. Chem. Phys. **35**, 1147 (1961); **37**, 993 (1962)
8. Podolsky, B., Pauling, L.: Phys. Rev. **34**, 109 (1929); Henneker, W. H., Cade, P. E.: Chem. Phys. Lett. **2**, 575 (1968); Epstein, I.R.: Chem. Phys. Lett. **9**, 9 (1971)
9. Abramowitz, M., Stegun, I. A. ed.: Handbook of mathematical functions. New York: Dover 1972

Received September 28, 1981